JOURNAL OF MATERIALS SCIENCE 27 (1992) 3843–3855

Interfacial properties of fibre-reinforced composites

C. Y. YUE*
School of Mechanical and Production Engineering, Nanyang Technological University, Nanyang Avenue, Singapore 2263
W. L. CHEUNG
Department of Mechanical Engineering, University of Hong Kong, Pokfulam Road, Hong Kong

Factors which control the strength and toughness of a fibre-reinforced composite in terms of the role of interfacial parameters such as the interfacial shear strength, the interfacial coefficient of friction and the matrix shrinkage pressure are reviewed. Techniques for determining the interfacial parameters, the stress distribution along the embedded fibre, and the mode of failure of the pull-out tests utilized in these techniques are considered.

1. Introduction

The study of interfaces in composite systems is considered essential to the development of an overall understanding of the science and technology of composites. There are two objectives in such studies of the interface: to understand the physical nature and character of the fibre–matrix interface and to determine how the interface affects the mechanical properties, and secondly to develop stress/fracture criteria to predict the debonding phenomenon and to characterize the composite in terms of interfacial parameters which control the strength and toughness of the composite.

The object of the present paper is to review the latter aspects of the interface. Issues such as the role of the interfacial parameters in the mechanical properties, the stress distribution along the embedded fibre and its effect on debonding, and techniques for evaluating the interfacial parameters will be considered. The single fibre pull-out test will be considered in detail as a review of the literature has shown that it is the only test which can potentially be utilized to determine certain interfacial parameters. Although aspects relevant to various fibre-reinforced composites are considered, the present review will focus on polymeric composites and include short-fibre systems.

2. Mechanical properties of composites

The strength, modulus, mode of failure and fracture toughness of a composite are not only dependent on the properties of the fibre and matrix, fibre volume fraction, fibre orientation and the embedded fibre length (in the case of short-fibre systems), but also on the interfacial parameters of the composite. Interfacial parameters include factors such as the interfacial shear strength τ_i, the interfacial toughness G_i, the matrix shrinkage pressure P_0 on the fibre, and the interfacial coefficient of friction μ. The influence of the above factors will be outlined.

2.1. Strength of composite

The theoretical strength of a short-fibre reinforced composite [1] is given by

$$\sigma_{cu} = C\left[\sum_i \frac{\tau_i l_i V_i}{2r} + \sum_j \sigma_{fu} V_j \left(1 - \frac{l_c}{2l_j}\right)\right] + \sigma_m(1 - V_f) \quad (1)$$

where σ_{cu} is the ultimate strength of the composite, σ_{fu} is the ultimate strength of the fibre, σ_m is the matrix stress at failure, τ_i is the interfacial shear strength, C is the orientation efficiency, l_c is the critical fibre length, l_i and l_j are the sub-critical and super-critical fibre lengths, respectively, V_i and V_j are the fibre volume fractions of the sub-critical and super-critical fibre lengths, respectively, V_f is the overall fibre volume fraction, and r is the fibre radius.

It can be seen from Equation 1 that the strength is affected by many parameters. The first two terms on the right of the above equation account for the varying short transfer lengths in short-fibre systems. In continuous fibre systems, the equation reduces to the simpler rule-of-mixtures relationship. It has been shown [2] for short-fibre systems that the reinforcement efficiency η of aligned short fibres increases with fibre length l. When $l/l_c > 10$, η approaches 95% of that of aligned continuous fibres (η approaches unity). It would therefore, seem that 95% of the strength of a continuous composite can be developed in a short-fibre composite provided $l/l_c > 10$. However, in practice, initiation of matrix failure at the fibre ends due to stress concentration severely reduces the strength of

*Author to whom correspondence should be addressed.

0022–2461

the composite. This has been confirmed using both acoustic techniques [3] and numerical finite-element methods [4]. It has also been shown [5] that badly damaged fibres will break into small fragments at relatively low stresses and reduce the strength and modulus of the composite.

The strength of the composite has been observed [6–8] to increase linearly with fibre volume fraction V_f as predicted by Equation 1. Systems with too high or too low V_f may deviate from this linear relationship due to fibre embrittlement of the matrix and fibre interaction, respectively. This phenomenon is more pronounced in a system with short fibre lengths and a weak fibre–matrix interface [8].

2.2. Toughness of composite

The toughness of a composite has been found [9–12] to be higher than that of the fibre or the matrix. One or more energy absorption processes which are not present in conventional materials must, therefore, exist in composite systems. The increase in toughness has been attributed to several fracture mechanisms. It has been proposed [13, 14] that work done against pull-out is a major contributor. Others [15] have considered the energy required to debond the fibre from the matrix to be a major factor.

Based on the above concepts, attempts have been made to improve the toughness without any sacrifice in strength in the composite. Most methods for increasing the toughness are based on promoting the occurrence of the fibre pull-out process. For example [16], fibres have been coated intermittently to produce alternating strong and weak bonding. The strong bonding maintains the required strength while the weak bonding assists crack blunting by the Cook–Gordon [17] debonding mechanism and increases the fibre pull-out length. There have also been attempts [18] to coat the fibres with a viscous fluid to maximize the shear stress acting on the fibres during pull-out. Such a shear stress is strain-dependent, and a faster strain rate causes a higher interfacial shear stress.

The benefits of using a "duplex" reinforcing member, consisting of a helical convoluted steel wire core shrunk in a hypodermic tubing, has also been investigated [19]. The strength of the hypodermic tubing controls the strength of the "duplex" reinforcing member. Once the hypodermic tubing has been loaded to fracture, the helical convoluted steel wire core will be pulled out against the inner wall of the tubing. The high frictional forces generated between the tubing and the helical steel core during the pull-out process lead to higher toughness. However, none of the above attempts has produced satisfactory practical solutions.

2.3. Role of interfacial parameters

The interfacial parameters have a significant effect on the properties of a composite. A weak interface drastically reduces the off-axis strength, the flexural strength [20] and the compression strength [20, 21]. The effect of water ingress on the properties of fibre-reinforced thermosetting polymers is well known. Water intrusion into the interface in an untreated short-fibre thermoplastic system [22] can also cause the strength and modulus to decrease by 70 and 80%, respectively. On the other hand, an increase in the interfacial strength leads to a substantial increase in the tensile strength and modulus of a short-fibre composite [8, 23].

The nature of the interface also has a large influence on the mode of failure and the toughness of the composite. Theoretical analysis based on the strain energy release rate [24] of the propagation of a penny-shaped crack in a composite has been conducted. Such an analysis showed that a strong interface would promote crack propagation across the fibres, whilst a weak interface would promote failure by fibre debonding and pull-out.

An increase in the interfacial shear strength τ_i is accompanied by a reduction in the critical fibre length l_c. Theoretical analysis of the fracture toughness [13, 14, 25] showed that the work done against pull-out increases with l_c and the frictional shear stress τ_f at the interface. The value of τ_f is governed by the matrix shrinkage pressure P_0 on the fibre and the interfacial coefficient of friction μ. The crucial effect of the above parameters on toughness has been emphasized by studies [26, 27] which indicated that fibre pull-out was by far the largest factor contributing to the fracture toughness of a fibrous composite.

2.4. Methods for evaluating the interfacial parameters

Although the interfacial strength has been evaluated from the stress–strain behaviour of a composite [1, 28], the results were strongly dependent on such factors as the specimen geometry, the fibre volume fraction and the fibre aspect ratio. The above analysis is based on a pull-out model which assumes a constant shear stress along the fibre [29]. However, in a short-fibre composite, the shear stress distribution is not constant due to the existence of a stress transfer length, stress concentrations arising from irregularly shaped fibre ends [30] and the interaction of the stress fields between adjacent fibres [31].

The principal techniques for determining the interfacial shear strength are the fragmentation test, the microindentation test and the pull-out test. The advantage of the pull-out test is that it is possible [32] to determine other interfacial parameters such as the interfacial coefficient of friction, μ, and the matrix shrinkage pressure, P_0, from the pull-out data. Hence, although each of the above tests will be considered, only the pull-out test will be evaluated in detail.

2.4.1. The fragmentation test

The interfacial shear strength is frequently evaluated by means of the fragmentation test [33]. This method is based [34] on the tensile pulling of a totally embedded single-fibre specimen in the direction of the fibre axis. Stress transfer between the matrix and the fibre

causes the tensile stresses along the fibre to build up. The tensile stresses are a maximum around the centre region of the fibre [35] beyond the transfer lengths of the system. Typically, the fibre fractures within this centre region during loading. Further increases in the tensile load will result in fragmentation of the fibre. When the length of the fibre fragments have reduced to a critical value, no further breakage will occur but the interface will fail in shear. If the fibre strength at the critical length L_c is known, the interfacial shear strength can be calculated from the average length of the fibre fragments l_a using the relationship

$$\tau_i = \frac{\sigma_{fu} r}{l_a} \Lambda(\rho) \quad (2)$$

where σ_{fu} is the fibre fracture strength, l_a is the average length of the fibre fragments, and $\Lambda(\rho)$ is a correction factor which can be estimated [36] using a Monte Carlo simulation.

However, it should be borne in mind that the strength of the fibre varies with its length [37]. The critical fibre lengths of some systems are so short [38] that direct measurement of their tensile strength is impossible. Although the problem of measuring the fibre strength at the critical length can be avoided by extrapolating the plot of fibre strength against fibre length obtained at practical lengths [34], the accuracy of the result is in doubt due to the lack of data at short fibre lengths. An alternative approach [36] is to utilize the Weibull–Poisson model to obtain the fibre fracture strength, σ_{fu}, such that

$$\sigma_{fu} = \sigma_{fu(l_0)} \left(\frac{l_a}{l}\right)^{\rho_0} \quad (3)$$

where ρ_0 is the shape parameter for fibre strength and σ_{fu} and $\sigma_{fu(l_0)}$ correspond to the Weibull scale parameters for the strength of the fibre at lengths l and l_0, respectively. The Weibull distribution $W(\sigma)$ of the fibre fracture strength of fibres of a given length l_0 is

$$W(\sigma) = 1 - \exp(-F^{\rho_0})$$

where $F = \sigma/\sigma_{fu(l_0)}$.

Most of the existing studies are limited to work on transparent matrix composites where the critical fragmentation lengths could be measured either directly optically or by using photoelastic techniques. More recently [39], the acoustic emission technique has been used to measure the fragmentation lengths in an E-glass epoxy and Kevlar epoxy systems. The use of acoustic emission will extend the applicability of the test to non-transparent systems.

The fragmentation test suffers from two main disadvantages. Firstly, the failure strain of the matrix must be much larger (more than three times) than the failure strain of the fibre to promote multi-fragmentation of the fibre. This requires the use of matrices which can undergo large deformations. Consequently, commercial resins utilized in actual composite systems which typically have low strains to failure cannot be used for the test. Therefore, the interfacial shear strength determined is not directly applicable to the actual composite system. Secondly, in addition to the difficulty of determining the fracture strength of very short fibre fragments, the strength and failure strain of the fibre may be affected [40] by the surrounding matrix. The coating or embedding matrix can inhibit fibre fracture [40] which initiate from surface flaws. The magnitude of this effect is dependent on the type of matrix or embedding resin. Therefore, it is important to utilize the actual fibre and resin of a given composite system to determine the interfacial shear strength τ_i.

The fragmentation test has recently been reviewed critically [41]. It has been shown [41] that Equation 3 is based on the assumption of a fully elastic model and is therefore not generally applicable to many practical composite systems. In addition, such an assumption is not realistic since the concept of a critical transfer length does not exist. Hence, theoretically, fragmentation would proceed and the fibre length would decrease as long as the applied strain on the specimen was increased. This is contrary to what is observed in practice. Instead, a partially elastic model [41], which accounts for inelastic deformations near the fibre ends, when the shear stress reaches either the yield strength of the matrix or the shear strength of the interface, must be utilized.

2.4.2. The microindentation test

In this technique, a pyramidal microhardness indenter is used to debond a fibre within a slice or section of composite material. The force from the indenter is applied directly to the fibre end. The indenter is fitted with an extensometer which serves as a load transducer. The measured debonding force could be used to calculate the interfacial shear strength by using a shear-lag model for push-out. This test was initially developed for fibre-reinforced ceramics [42, 43] but has been extended to other fibre–matrix systems. Detailed finite-element analysis of the test has also been done [43]. Highly automated systems for testing, data acquisition and analysis are available [44]. This technique has also been reviewed elsewhere [41].

When a thin slice of composite is used, the push-through test is obtained. The push-through test has been used to investigate the effect of silane coupling agents on the interfacial shear strength in E-glass epoxy systems [45]. The use of acoustic emission methods [45] to detect the onset of debonding has also been attempted. However, large-amplitude emissions which can be attributed to crack formation in the fibre during push-out have made interpretation of the acoustic emission data rather difficult.

The advantage of the microindentation test is that practical composites can be sliced and tested. However, accurate interpretation of data from tests in which the fibres are not aligned vertically is a problem. This is because the relative frictional sliding resistance is dependent on the fibre alignment. Discernment must also be exercised in selecting the fibres for the test, since fibre bundle effects within the sliced composite would also contribute to scatter in the results.

2.4.3. The pull-out test

The single-fibre pull-out test is by far the method most commonly employed for determining the interfacial parameters. The pull-out test will be evaluated in detail in a later section. Pull-out tests have been performed on many systems including the steel wire–rubber matrix [46–48], the steel wire–cement matrix [49–51], the glass fibre–cement matrix [52], the polypropylene fibre–cement matrix [53], the metal fibre–epoxy matrix [54–56], the glass fibre–thermosetting plastic matrix [57], the steel wire–polycarbonate matrix [55] and the glass fibre–polypropylene matrix [58] systems.

The microbond test [59] is essentially a miniature pull-out test. In this test, droplets of resin are allowed to cure or solidify on small fibres which are available commercially. The resin is supported and the fibre is pulled through the resin droplet. The interfacial shear strength is determined from the pull-out force. The attractiveness of the microbond method lies in the simplicity of the specimen preparation. However, there are a number of disadvantages. The resin droplets must necessarily be small (compared with the critical length), otherwise fibre fracture would occur readily. Other considerations include the fact that the shape (usually ellipsoid) of the droplet is important since droplet shapes which deform excessively would not lend themselves to accurate analysis. This method is not applicable to matrices which are soft. Moreover, the interfacial shear strength is calculated on the assumption that the stress is distributed uniformly at the interface. The microbond test will not be considered in detail in this review.

In contrast to the fragmentation test and the microindentation test which can only determine the interfacial shear strength, the single-fibre pull-out test has been used to evaluate at least four interfacial parameters. These parameters include the interfacial shear strength τ_i [51, 57], the interfacial fracture toughness G_i [57, 60], the matrix shrinkage pressure P_0 [58] and the interfacial coefficient of friction μ [54, 55, 61]. There is little work on glass fibre-reinforced thermoplastic systems despite the fact that this class of composites has great technological importance [62].

Most pull-out tests utilize fibres of constant diameter, and different interfacial parameters are evaluated [57, 60] from tests with different geometry and test configuration. For example, the matrix shrinkage pressure of epoxy on glass fibre can be determined [63] using photoelastic methods. However, such a method for determining P_0 is limited to photoelastic materials only. In contrast, a recent method [58] for determining the interfacial parameters involves the pull-out testing of slightly tapered glass fibres. The latter technique allowed assessment of the interfacial parameters from one type and set of pull-out tests.

2.4.4. Comparison of data from different methods

In the absence of a standard for determining the interfacial shear strength, the reliability, reproducibility and consistency of results from different workers obtained for a given composite system utilizing a given technique must be examined. The paucity of data does not allow the newer microindentation test to be evaluated. It has been reported [64] that there is general to fair agreement of data from fragmentation tests on carbon AS4–epoxy systems and carbon AS4–PEEK systems. Less satisfactory agreement was reported for pull-out data for untreated HT carbon–DGEBA systems. It was reported [64] that the interfacial shear strengths determined from pull-out tests were dependent on the mode of stress application. This observation will be outlined and explained in a latter section. Hence, it is imperative that the mode of loading must be similar for pull-out data to be comparable and consistent.

It is also important to know whether data obtained from the different methods are comparable for a given composite system. Comparison of data from pull-out, fragmentation and microindentation tests on Kevlar, E-glass and carbon systems [65] revealed that only qualitative comparisons can be made. In contrast, agreement between data from pull-out and fragmentation tests has also been reported by Jacques [64]. Clearly, more work must be done before any firm conclusion can be drawn. Any comparison of data from the different methods would also be affected by the appropriateness of any assumption made in calculating the value of τ_i. The consequence of comparing τ_i obtained from the fragmentation data with large fragmentation lengths and τ_i obtained from pull-out tests will be highlighted.

3. Stress distribution along the fibre

3.1. Introduction

Apart from the intrinsic properties of the interface or interphase, the stress distribution along the embedded fibre also plays an important role in the overall performance of the composite. Regions of shear stress concentration will develop at the interface because of the differing properties of the fibre and matrix. Shrinkage pressure also develops at the interface on curing or cooling of the matrix, as a result of differential shrinkage due to a difference in thermal expansion coefficients of the two constituents.

The stress distributions along a short fibre are strongly influenced by the properties of the fibre and matrix, and the interface or interphase. Stress concentrations near the fibre ends can cause partial debonding of the interface or shear flow of the matrix. In the case of randomly oriented fibre composites, fibre misalignment and interaction due to overlapping of neighbouring fibres complicate the stress distribution further.

A number of theories have been put forward to predict the stress distribution along the fibre. Most of these are based on the shear lag principle. Results from experimental approaches suggest that most theories provide a good fit in the middle section of the fibre but underestimate the magnitude of stress concentration near the fibre ends. Nevertheless, these theories are

very useful in the development of an understanding of stresses along the fibre.

3.2. Theoretical pull-out models

The shear lag theory was initially utilized by Cox [35] to determine the stresses along a discontinuous fibre embedded in a matrix. The fibre and the matrix were assumed to be elastic. The bond between the fibre and the matrix was assumed to be perfect and load transfer through the fibre ends was neglected. When such a system containing a fibre of length l is stretched to a strain ε, the load transferred from the matrix to the fibre at any distance x from the fibre end can be written as

$$\frac{dP}{dx} = H(u - v) \quad (4)$$

where P is the load on the fibre, u the displacement of a point on the fibre–matrix interface under the applied load, v the displacement at the same point in the absence of the fibre, and H [66] is $2\pi G_m/\ln(r_m/r)$ where G_m and r_m are the shear modulus and radius of the matrix, respectively. It can be shown that the expressions for the tensile stress along the fibre σ_f, and the shear stress at the interface τ_x, are given by

$$\sigma_f = \frac{(E_f - E_m)\sigma_c}{E_m}\left(1 - \frac{\cosh\{\beta[l/2 - x]\}}{\cosh(\beta l/2)}\right) \quad (5)$$

$$\tau_x = \frac{(E_f - E_m)A_f\varepsilon}{2\pi r}\left(\frac{\beta\sinh\{\beta[l/2 - x]\}}{\cosh(\beta l/2)}\right) \quad (6)$$

where A_f is the cross-sectional area of the fibre and $\beta = (H/A_f E)^{1/2}$.

The above model assumes excellent adhesion between the fibre and the matrix. This, however, is not true for some fibre-reinforced thermoplastic systems. In such systems [67], a poor interfacial bond exists and high stresses at the fibre ends would cause interfacial debonding. Load transfer is, therefore, due to friction induced by any relative movement between the fibre and the matrix. The tensile stress along the debonded fibre can readily be determined where

$$\sigma_f = \frac{2\mu P_0}{r}x \quad (7)$$

where x is the distance from the fibre end.

The above models do not account for deformation of the matrix away from the interface which may have an effect on the stress transfer. Dow [68] proposed a model similar to that by Cox [35], but assumed no contact with the matrix at the fibre ends. In addition to the assumptions in Cox's analysis, Dow assumed that the displacement of the matrix along the fibre direction increased linearly with the perpendicular distance from the axis of the fibre. The expressions for σ_f and τ_x become

$$\sigma_f = \frac{P_m}{A_f + (A_m E_m/E_f)}\left(1 - \frac{\cosh(\lambda x/d_f)}{\cosh(\lambda l/d_f)}\right) \quad (8)$$

$$\tau_x = \frac{\lambda}{4}\frac{P_m\sinh(\lambda x/d_f)}{[A_f + A_m(E_m/E_f)]\cosh(\lambda l/d_f)} \quad (9)$$

where P_m is the load on the matrix, A_m is the matrix cross-sectional area, d_f is the fibre diameter, $2l$ is the fibre length, x is the distance along the fibre axis measured from the mid-point of the fibre, and

$$\lambda^2 = 4\left(\frac{2^{1/2}(G_f/E_f)[1 + (A_f E_f/A_m E_m)]}{(2^{1/2} - 1) + (G_f/G_m)\{[(A_m/A_f) + 2]^{1/2} - 2^{1/2}\}}\right)$$

It has been suggested that an "interphase" layer which has the "average" properties of the composite may form on the fibre surface. A model which accounts for the presence of such an interphase has also been developed [69]. Three assumptions were made in this model. Firstly, perfect bonding at the fibre–interphase and matrix–interphase interfaces was assumed. Only the fibre and interphase were load-bearing, and the matrix layer was assumed to carry only shear stress. Based on these considerations, the expressions for the tensile stress on the fibre σ_f and the shear stress at the interphase–matrix interface τ_x are

$$\sigma_f = \frac{\sigma_c r_a^2 E_f}{E_a(r_a^2 - r_m^2) + E_f r^2}\left(1 - \frac{\cosh(\eta_0 x)}{\cosh(\eta_0 l)}\right) \quad (10)$$

$$\tau_x = \frac{G_m\sigma_c r_a^2\sinh(\eta_0 x)}{\eta_0 E_a(r_m - r)(r_a^2 - r_m^2)\cosh(\eta_0 l)} \quad (11)$$

where

$$\eta_0^2 = 2\left[\frac{G_m}{E_m(r_m - r)r}\left(1 + \frac{E_f}{E_a}\frac{r^2}{(r_a^2 - r_m^2)}\right)\right]$$

E_a is the modulus of the average material and r_a is the outer radius of the average material block.

The above theories are concerned with stresses within an elastic matrix. However, in some systems the matrix may be in a plastic state. In the latter case [29], shear flow of the matrix is assumed to occur when the interfacial shear stress reaches the yield stress of the matrix. This initial analysis was developed for a copper matrix which had a very low yield stress so that the matrix could be considered to be totally plastic. The shear stress at the interface was, therefore, constant and equal to the shear strength of the matrix τ_{mc}. The tensile stress on the fibre σ_f can readily be shown to be

$$\sigma_f = 2\tau_{mc}\frac{x}{r} \quad (12)$$

In some composite systems of stiff fibre in a metal matrix of low yield stress, plastic flow of matrix at the interface will occur near the fibre ends while the matrix in the middle section remains elastic. Therefore, both the above theory [29] and Cox's theory [35] can each describe only part of the interfacial

stress distribution in such a system. These two theories can, however, be combined and extended [70] to include the load transferred at the fibre ends. In such a model, the tensile stress on the fibre σ_f in the region where the matrix is still in an elastic state consists of three parts: (i) a step increase across the fibre ends, (ii) a linear increase due to shear flow of matrix near the fibre ends, and (iii) an exponential increase in the form similar to Cox's theory [35] in the middle section of the fibre. The expression for stress in the fibre becomes

$$\sigma_f = \sigma_m + \frac{2l_p\tau_m}{r} + \frac{2\tau_m}{\beta r}\left(1 - \frac{\cosh(\beta x)}{\cosh[\beta(L - l_p)]}\right) \times \coth[\beta(L - l_p)] \quad (13)$$

where $\sigma_m = 2\tau_m$, $2L$ is the embedded fibre length, l_p is the length of the shear flow region, x is the distance along the fibre axis as measured from the centre of the fibre, $\beta^2 = H/E_f\pi r^2$, and H is the constant in Cox's equation.

3.3. Comparison of the theories

Three of the above theories, Equations 4 [35], 8 and 9 [67], and 10 and 11 [69] are based on the shear lag principle. These theories can be summed up by two general equations for σ_f and τ_x where

$$\sigma_f = K_1\left(1 - \frac{\cosh\{[(l/2) - x]K_2\}}{\cosh[(l/2)K_2]}\right) \quad (14)$$

$$\tau_x = K_3\left(\frac{\cosh\{[(l/2) - x]K_2\}}{\cosh[(l/2)K_2]}\right) \quad (15)$$

The constants K_1, K_2 and K_3 are different for each theory due to the different assumptions made and minor differences in the configuration of the models.

Similarly, Equations 7 and 12 are of the same form. However, the former considers the constant shear stress to be due to the interfacial friction which arises from ineffective bonding, while the latter attributes the constant shear stress to shear flow of the matrix.

All the above theories were developed for unidirectional short-fibre reinforcement. Very often, short-fibre reinforced thermoplastics with randomly oriented fibres are developed in order to achieve isotropic mechanical properties. If a fibre is not oriented parallel to the applied load, the stress distribution can be very different [71].

Interfacial stress distributions have also been analysed experimentally using different techniques. For example, resonance Raman spectroscopy [72] has been utilized to measure the strain distribution along a single-crystal polydiacetylene (PDA) fibre in a uniaxially loaded single-filament model composite of PDA in epoxy. The Raman technique has also been used to characterize carbon fibres [73] and for mapping the load transfer profiles from fibre ends in PBT–epoxy [74] and aramid–epoxy [75] systems. The results from the fully embedded fibres agreed qualitatively with Cox's theory. However, the stress distribution [73] around the broken fibre fragments did not conform to the profile predicted by Cox. This also brings into question the accuracy of the interfacial shear stress calculated using the fragmentation method which is based on the assumption of a shear-lag analysis.

Most theoretical analyses [35, 68, 69] ignore the load transferred across the fibre ends. This leads to an underestimation of the stress concentration at the fibre ends. Finite-element analysis has shown [76, 77] that load transfer increases the stress concentration at the fibre ends by more than 20%. The distribution of stress at the fibre ends is also dependent on the geometry of the fibre tip [76], and a gradually tapered end reduces shear stress concentration.

The photoelastic technique is another method for determining the interfacial stress distribution experimentally. Such work on a two-dimensional model of aluminium fibre in an epoxy resin [30] revealed that the magnitude of the interfacial shear stress at the fibre ends was three times higher than that predicted from Cox's theory. Nevertheless, away from the fibre ends, the theory predicted values close to the experimental results. Similar photoelastic experiments on a model system of boron fibre in an epoxy system [31] revealed that residual shrinkage stresses in the matrix reduce the stress concentration although they may affect the load transfer. In a multi-fibre model system, the stress concentration is greatly affected by interaction between adjacent fibres. Intermediate overlapping seems ideal for reducing interfacial stress concentration. However, very high stress concentration arises when the regions of high stress are brought into close proximity. Similar results from a theoretical viewpoint have also been obtained [78].

It has been shown [79] that a change in the shape of the fibre tip affects the position of maximum stress but has little effect on the overall stress distribution. The point of maximum stress concentration in a square-ended fibre system is located at a short distance from the fibre end, whilst that in a round-tip fibre system is at the fibre tip. However, there is little scope for improvement in this particular aspect since the shape of the fibre ends in real composite systems cannot be controlled.

3.4. Other considerations

Interphases in composites will also affect stress transfer and thus the interfacial stress distribution in composites. The interface and interphase of a fibre-reinforced composite are physically different in nature. The former is the boundary at which the reinforcement and the matrix meet, while the latter is either a layer of matrix material which has a different morphological structure from the bulk matrix due to the presence of the fibre surface, or a layer of mixed material of two phases which are in contact at the fibre surface. The latter type of interphase exist in commercial composites since the fibres normally have either a protective coat of binder (or sizing) or a coat of silane coupling agent. As the fibre and the matrix material interact through the coating on the fibre, the properties of the coating will affect the microscopic and macroscopic properties of the composite. The

subject of binder coatings and coupling agents is outside the scope of the present review.

The interphases cited in the literature generally consist of a fairly distinct coat of binder/sizing [80–82] or coupling agent [83] on the fibre. It has been recognized [84] that some inter-diffusion may occur at the coating–matrix interface so that the interphase region is diffused and larger than the original thickness of the coating on the fibre. However, the exact nature of the interphase may be more complex [85]. Most of the existing work on interphases concerns epoxy or other thermosetting polymer matrix systems.

The interphases in thermoplastic fibre composites are the transcrystalline regions which develop on the fibre surface. Such transcrystalline interphases have been observed in carbon fibre–nylon 6 and glass fibre–nylon 6 systems [86], Kevlar–polypropylene [87], Kevlar–nylon 66 [88], glass fibre–HDPE [88], and glass fibre–PPS and carbon fibre–PPS systems [89]. Most of the above studies were done on a hot stage. It is important to treat hot-stage results with care since transcrystalline growth which was present in hot-stage studies on carbon fibre–nylon 66 and Kevlar fibre–nylon 66 systems [88] did not exist in the injection-moulded samples. This was observed despite the fact that transcrystalline growth does occur in injection mouldings.

A different type of interphase in thermoplastic systems has been reported [90] in both clean glass fibre–polypropylene composite and silane-treated glass fibre–polypropylene composite. The interphase region in the above silane-treated glass fibre–polypropylene composite contained two distinct layers. A distinct layer of interphase material existed on top of the silane layer on the treated glass fibre. Hence, interfaces existed between the glass fibre–silane, silane–interphase and interphase–polypropylene layers. This is the first time [90] that a physically distinct layer of interphase material other than the transcrystalline layer has been reported in the literature. Transcrystalline growth also existed [90] in the water-quenched samples. None of the existing models accounts for the presence of so many layers and interfaces in the interface region.

The presence of silane agglomerates on the treated fibre surface [90] may further affect the microstress distribution in the interface region. Shrinkage artefacts [91] at the interface in reinforced thermoplastics with poor adhesion between the fibre and the matrix also change the nature of the interfacial stress distribution.

4. The single-fibre pull-out test

4.1. Introduction

The pull-out process in composites makes a large contribution to its toughness [9, 13, 25]. This has encouraged attempts to improve the toughness by promoting the pull-out process during failure, and efforts to understand the dynamics of the pull-out process through the single-fibre pull-out test. The dynamics of the pull-out process and the work done against the frictional stress during fibre pull-out are greatly influenced by interfacial parameters such as the interfacial shear stress τ_i, the interfacial fracture energy G_i, the interfacial coefficient of friction μ, and the matrix shrinkage pressure P_0 on the fibre.

The single-fibre pull-out test is most extensively used for studying the dynamics of the pull-out process because of its simplicity (there are fewer unknown factors than in a real composite system, and the single-fibre pull-out curve shows distinct regions of the pull-out process) and versatility (can be used to evaluate a number of interfacial parameters). Various theories have been developed to predict the load required to debond the fibre from the matrix in a single-fibre pull-out test. These theories are either based on the maximum interfacial shear stress criterion or on the interfacial fracture energy criterion.

4.2. Test configuration

A typical single-fibre pull-out test specimen usually consists of a fibre partially embedded in a block of matrix as shown schematically in Fig. 1. The protruding end of the fibre is gripped and pulled during testing. The test can either be performed with the matrix supported at the fibre emergent end (position A in Fig. 1) or at the opposite end to the fibre (position B in Fig. 2). Usually there is a certain fibre free length L_f (see Fig. 1) between the matrix and the grip. In the case where $L_f = 0$, the fibre is said to be fully supported. It is important to maintain a small and constant L_f. If L_f is large, the release of stored elastic energy in the fibre due to reduction in the stress immediately after debonding will make a large contribution to pull-out of the fibre. This has to be taken into account in the ensuing analysis. A very large L_f may sometimes lead to catastrophic debonding.

4.3. Characteristics of the pull-out curve

The plot of pull-out force F_p versus displacement x of a stiff fibre in a polymeric matrix generally consists of three parts [55, 92, 93] as shown in Fig. 2. This includes (i) region I, where F_p increases linearly up to a maximum value F_d at which complete debonding of the fibre occurs; (ii) region II, where a sharp drop of F_p from F_d is followed by a few oscillations due to stick and slip of the fibre; and (iii) region III, where the force sustained by friction gradually decreases as the fibre is progressively pulled out.

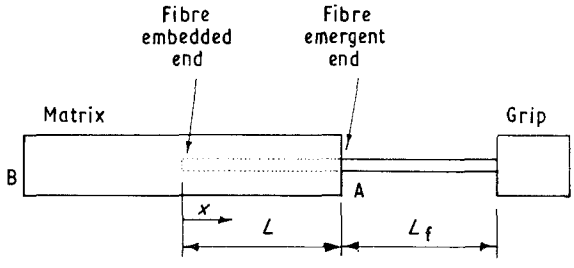

Figure 1 Schematic representation of a single-fibre pull-out test specimen (fibre diameter = $2r$, matrix block diameter = $2r_m$).

TABLE I Summary of theoretical models

Model	Shear stress distribution	Constant
I	$\tau_x = \frac{\alpha_1 F_p}{2\pi r}\left(\frac{\cosh(\alpha_1 x)}{\sinh(\alpha_1 L)}\right)$	$\alpha_1 = \left(\frac{2G_i}{b_i r E_f}\right)^{1/2}$
II	$\tau_x = \frac{\alpha_2 F_p}{2\pi r}\left(\frac{\cosh(\alpha_2 x)}{\sinh(\alpha_2 L)}\right)$	$\alpha_2 = \left[H\left(\frac{1}{A_f E_f} - \frac{1}{A_m E_m}\right)\right]^{1/2}$
III	$\tau_x = \frac{\alpha_3 F_p}{2\pi r}\left(\frac{\cosh(\alpha_3 x)}{\sinh(\alpha_3 L)}\right)$	$\alpha_3 = \left(\frac{H}{A_f E_f}\right)^{1/2}$

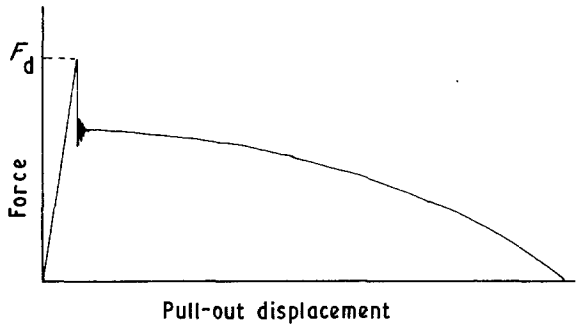

Figure 2 General characteristics of the load–displacement curve for a single-fibre pull-out test.

In some systems, the interface remains intact and debonding initiates and propagates rapidly to cause complete debonding of the interface at the end of region I. In other systems, such as the silane-treated glass fibre–polypropylene system [94], the debonding crack initiates around the half-way point and propagates within this region. Region II is a transition region where the maximum force for complete debonding F_d reduces to a value required to extract the debonded fibre from the matrix. A relaxation in strain energy in the matrix and fibre accompanies this reduction in force. The striations or oscillations in region II are due to stick and slip between the fibre and the matrix during the transition from a crack debonding phase to a pull-out phase, which occurs while the specimen is being strained in the testing machine.

The size of each of these regions is dependent on the interfacial parameters of the composite system under consideration. Systems with a higher interfacial shear strength τ_i will have a plot with a steeper slope in region I and a larger F_d will be obtained. Composite systems in which the frictional shear stress τ_f (stress between the debonded fibre and the matrix during fibre extraction) is only slightly lower than τ_i will exhibit a very small drop in region II. This has indeed been observed [95] in a glass fibre–polypropylene system. Composites with higher values of either P_0 or μ will have a region III of larger area, which can be attributed to greater work done against frictional pull-out. Such composites have an increased toughness. Therefore, the change in shapes and sizes of regions I, II and III gives an indication of the way in which τ_i, τ_f, P_0 and μ vary between different composite systems.

TABLE II Parameters for a glass fibre–polypropylene system

E_m (GPa)	E_f (GPa)	ν_m	ν_f	r_m (mm)	r (mm)	L (mm)
3.4	70	0.35	0.22	2.5	0.3	10

4.4. Longitudinal interfacial shear stress distribution

A knowledge of the shear stress distribution along the fibre embedded length in a single-fibre pull-out specimen is important, since the debonding crack initiates at the position where the shear stress approaches the interfacial shear strength. Some previous work [93, 96, 97] has utilized Cox's [35] shear lag principle to determine the stress distribution along a totally embedded fibre. In order to facilitate comparison, the above three theories were re-derived using the notations shown in Fig. 1. The results are as listed in Table I where H is the constant in Cox's analysis, b_i is the effective thickness of the interfacial region, G_i is the shear modulus of the interfacial region, r_m is the radius of the matrix block, G_m is the shear modulus of the matrix, and A_m and A_f the cross-sectional area of the matrix and fibre, respectively.

It can be seen from Table I that the equations from the above theories have exactly the same form and differ only in their constant terms α_1, α_2 and α_3. Consider a system which has the parameters shown in Table II under a pull-out force of 10 N. The theoretical interfacial shear stress distributions predicted by the above theories are as shown in Fig. 3. It can be seen from Fig. 3 that theory I predicts the highest stress concentration while the results from theories II and III are similar.

4.5. Debonding crack initiation

It can be seen from Fig. 3 that all the above three theories predict that the debonding crack will initiate at the fibre emergent end, since they predict a maximum shear stress concentration at $x = L$. The debonding crack will then propagate towards the fibre embedded end. This is true if the pull-out test is executed with the matrix block supported at the fibre emergent end [92].

However, debonding has been reported to initiate at both the fibre emergent end and at the fibre embedded end when the pull-out test is performed by gripping the opposite end of the specimen. For example, crack

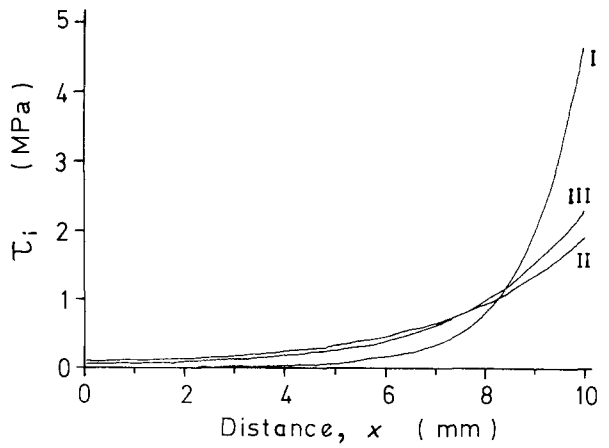

Figure 3 Interfacial shear stress distribution for a glass fibre–polypropylene system based on models I, II, and III in Table I.

initiation has been observed at the fibre emergent end in a nickel wire–epoxy system [56], while debonding crack initiation at the fibre embedded end has been reported in a steel cord–rubber model [98]. Furthermore, a two-stage debonding process has been reported [99] in a glass fibre–epoxy system where the debonding crack first initiated at the fibre embedded end. This was followed by initiation of a second debonding crack at the fibre emergent end. The above observations imply that the point of interfacial shear stress concentration depends not only on the testing configuration but also on the properties of the fibre and the matrix.

4.6. Maximum interfacial shear stress criterion for debonding

The debonding force, F_d, required to extract a stiff metal wire from a soft metal matrix [29] has been observed to be a linear function of the embedded length, L, of the wire. This is in agreement with separate work [100] on a phosphor-bronze wire–plasticized epoxy system. The shear stress along the fibre embedded length in the above system was assumed to be constant, due to shear flow of the soft metal matrix and to the relatively constant shear strain of the rubber matrix. The slope of the plot of F_d against L was considered to be the strength of the interface, τ_i, where

$$\frac{dF_d}{dL} = 2\pi r\tau_i \tag{16}$$

In the case of elastic matrices, however, the shear stress distribution varies along the fibre embedded length L [93, 96, 97, 101] so that Equation 16 is not applicable. The relationships between F_d and L derived from theories based on the maximum shear stress criterion have been reviewed elsewhere [102]. Sometimes [96, 101] catastrophic complete debonding occurs immediately after the debonding crack has initiated at the region of maximum stress concentration. In such a situation, the pull-out force for complete debonding is given [101] by

$$F_d = \frac{2\pi r\tau_i}{\alpha}\tanh(\alpha L) \tag{17a}$$

where $\alpha = (2H/rE_f)^{1/2}$ and H is the constant in Cox's analysis. Equation 17a can be rearranged to give

$$\tau_i^{max} = \frac{\tau_i \tanh(\alpha L)}{\alpha L} \tag{17b}$$

where $\tau_i^{max} = F_d/2\pi rL$ is actually the average stress on the fibre.

It can be seen from Equation 17a that F_d increases rapidly at small L but levels off to a constant value, $F_d = 2\pi r\tau_i/\alpha$, as l is increased further. This implies that complete debonding can take place even when L is very large provided that the ultimate tensile strength of the fibre is higher than $2\pi r\tau_i/\alpha$.

The magnitudes of τ_i and τ_i^{max} have been determined [103] for two carbon fibre–epoxy systems using a fully supported fibre specimen configuration (where one end of the fibre is embedded in the matrix block). The value of τ_i^{max} was dependent on the embedded length l and approached τ_i when l was very small ($l < 30$ μm) [103]. The interfacial shear strength τ_i for the two composite systems was 123.9 and 174.2 MPa, respectively, while τ_i^{max} (for $l > 200$ μm) was 15 and 12 MPa, respectively. This compares with τ_i values of 15 to 26 MPa utilizing the fragmentation method (fibre fragment lengths of 280 to 1700 μm), and τ_i values of 9 to 55 MPa from the pull-out method (pull-out lengths of 60 to 400 μm) as obtained by other workers [103] for similar carbon-fibre systems. The above results suggest that accurate values of τ_i can only be obtained if the fragmentation lengths and pull-out lengths are very small ($l < 30$ μm in this case). Otherwise, the interfacial shear strength values determined are really τ_i^{max}. Such work has to be extended to other composite systems. Nevertheless, the work [103] indicates that τ_i is more likely to be determined from pull-out tests and that due consideration has to be given to the fibre embedded lengths and fibre aspect ratios used.

Debonding can also be considered a gradual process such that the interfacial friction in the debonded area can be taken into account [52, 97]. Such analysis assumes that debonding will initiate at the position where the shear stress approaches the shear strength of the interface. An increase in the pull-out force, F_p, will cause the debonding crack to propagate and create a debonded region. As the debonded crack continues to propagate, the bonded area will decrease while the debonded area will correspondingly increase. Consequently, the resistance against pull-out due to the bonded region will decrease while the frictional force generated in the debonded region increases.

In systems where the fibre embedded length is long and at the early stage of any debonding process, the increase in friction in the debonded area will be greater than the drop in load-bearing capacity in the bonded region. Therefore, the total resistance against pull-out will increase as the debonding crack propagates. The debonding crack grows under the action of the applied load, and crack propagation will stop when the total resistance against pull-out is in equilibrium with F_p. Further increases in F_p are necessary to cause propagation of the debonding crack.

4.7. Interfacial fracture energy criterion for debonding

The debonding process can also be considered in terms of the energetics of failure [15, 104, 105]. Debonding crack propagation takes place when the fibre strain energy at the debonding crack front is higher than the fracture energy of the interface, G_i. In order to maintain crack propagation, the fibre tensile stress, σ_d, at the crack front must remain at

$$\sigma_d = \left(\frac{4E_f G_i}{r}\right)^{1/2} \quad (18)$$

The principle of conservation of energy was utilized in a study [48] of the debonding of steel cord from a rubber matrix. The total energy in the above pull-out system before debonding was assumed to consist of two parts: (i) the tensile strain energy in the unreinforced part of the fibre (i.e. the region between position B and the fibre embedded end as in Fig. 1), and (ii) the stored energy in the loading device. When a length of steel cord had debonded, the corresponding volume of rubber was assumed [48] to be in simple tension. This gives rise to an increase in strain energy in the rubber. On the other hand, such an extension in the debonded region of the rubber will cause a drop in strain in the loading device and hence a reduction in the stored energy. The decrease in stored energy in the loading device was found to be exactly twice as large as the increase in strain energy in the rubber. The difference in the above two energy terms was taken to be the fracture energy of the interface. The debonding force F_d was independent of the embedded length, L, of the cord and was given by

$$F_d^2 = 4\pi(A_m - \pi r^2) r E_m G_i \quad (19)$$

Although the experimental results [48] revealed that F_d did remain reasonably constant at long steel cord embedded lengths L, F_d decreased with decreasing L for short steel cord embedded lengths ($L < 15$ mm, steel cord radius of 0.76 mm).

A different approach was taken in a separate study [57] on the glass fibre–epoxy system. From a consideration of the balance of the total strain energy in the embedded fibre length and the interfacial energy, the debonding force F_d was found to increase with increasing fibre embedded length L. The rate of increase in debonding force F_d decreased as L increased such that

$$F_d = 2\pi r(G_i L E_{fm})^{1/2} \quad (20)$$

where

$$E_{fm} = \left(\frac{E_f E_m}{(1 + \nu_m)\ln(r_m/r)}\right)^{1/2}$$

and ν_m is the Poisson's ratio of the matrix. According to the above model [57], the strain energy in the fibre embedded length should reduce to zero and the fibre should be in a stress-free state at complete debonding. However, contrary to the above predictions, the pull-out force did not drop to zero in the experiments [57]. Hence, the analysis is suspect.

The debonding process has also been considered [106] utilizing the Griffith-type criterion for crack growth. Such studies revealed two distinct situations. In a system with a long elastic fibre, steady crack growth would take place under a constant load. In systems with either a rigid fibre or a short embedded fibre length, once the debonding crack has initiated, it will propagate catastrophically until complete debonding.

Other workers [107] have utilized different failure criteria for different failure modes. In the ductile mode, debonding was assumed to occur when the shear stress at the interface approached the shear strength of the matrix. The idea that the shear stress along the fibre was constant due to shear flow of the ductile matrix was also adopted [29]. On the other hand, the energetic failure criterion was applied where failure was in the brittle mode. It was demonstrated [107] that increasing the fibre diameter could cause a transition from ductile to brittle behaviour. A recent method [108] for selecting either a strength-based or fracture-based approach for the analysis of fibre debonding which assumes the existence of a transition zone has been proposed. This transition is assumed to exist between the elastic bonded zone and the debonded frictional zone and is postulated to be a region where breakdown of material takes place.

4.8. Other factors which affect debonding

Uncharacteristic load–displacement plots for the pull-out of a nickel wire from an epoxy matrix and from a cement-based matrix have been reported [56]. A typical reported curve is shown in Fig. 4. Provided the wire is long enough, it can be seen from Fig. 4 that the typical rapid drop in pull-out force no longer exists. Instead, the pull-out curve exhibits a plateau of debonding force. This plateau corresponds to the yielding of the nickel wire. Since the maximum tensile stress is on the free length of the wire, plastic yielding will start there. After the free length has completely yielded and work-hardened, yielding will extend progressively inward into the pull-out specimen. The radial contraction arising from longitudinal straining causes the wire to separate and lose contact with the matrix. The debonding crack front ahead of the yielded zone in the nickel wire will thus travel under a constant load, giving rise to the debonding plateau.

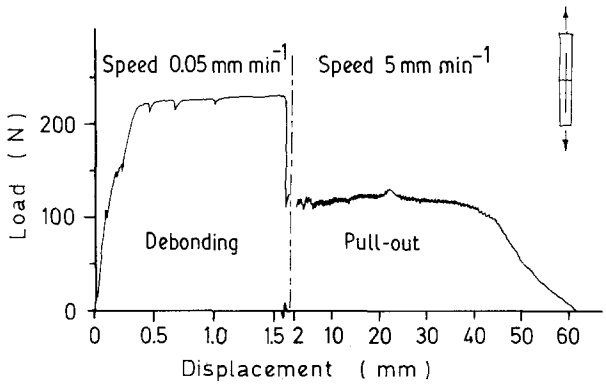

Figure 4 Load–displacement curve of a single fibre pull-out test in a nickel wire–epoxy system [48].

The load required to debond a fibre, F_d, is also affected by a change in radial pressure on the fibre. An increase in F_d has been reported following the direct application of hydrostatic pressure on the matrix [54, 60]. The interfacial shear strength approached the shear strength of the matrix [54] when the external hydrostatic pressure was high.

4.9. Effect of μ and P_0 on pull-out

After complete debonding, the shape of the pull-out curve is governed by the interfacial friction τ_f. The value of τ_f is dependent on the radial pressure, P_0, on the fibre and the interfacial coefficient of friction μ. If μ is constant and the Poisson contraction of the fibre is insignificant, the pull-out force F_p which acts against friction is a linear function of the pull-out displacement x such that

$$F_p = 2\pi r\tau_f(L - x) \quad (21)$$

where

$$\tau_f = P_0\mu \quad (22)$$

In practice, the value of τ_f should not change during pull-out. However, τ_f has been reported [109] to decrease when an epoxy matrix was used. It has been suggested that this decrease may be due to the lower modulus of the deformed matrix and an increase in temperature during the pull-out process. If the matrix is metallic [29] and not polymeric in nature, work-hardening of the deformed matrix will lead to an increase in τ_f.

4.10. Effect of fibre shrinkage on pull-out

Poisson shrinkage at the fibre emergent end becomes significant when the fibre tensile stress is high. Such high tensile stresses may develop in systems where the embedded fibre length is large and are more pronounced in ductile fibre systems. The fibre shrinkage leads to a decrease in the effective matrix shrinkage pressure on the fibre around the fibre emergent end. This effect was accounted for in some of models [93, 110] which showed that the rate of increase in pull-out stress acting against friction decreased as the fibre embedded length increased. It is interesting to note that theoretically [56, 93], a fibre of indefinite (large) length can be extracted from the matrix provided that alignment is perfect. The Poisson contraction effect diminishes as pull-out progresses due to the lower force required for pull-out, and the consequent decrease in tensile stress on the fibre. This is reflected [60, 92] in the increasing slope of the force–displacement plot.

4.11. Determination of μ and P_0

The value of τ_f can be determined from the slope of the frictional pull-out curve and Equation 21. If the Poisson contraction in the fibre is pronounced, the slope at $x = L$ must be used instead, since at this point the fibre stress is zero and the Poisson effect becomes non-existent [93]. However, the task of separating τ_f into P_0 and μ remains. This could be overcome by performing the single-fibre pull-out test while subjecting the matrix to different external hydrostatic pressures P_a [54, 60]. It has been shown that when P_a is less than the shear yield strength of the matrix, τ_f is a linear function of the external hydrostatic pressure and Equation 18 can be modified as

$$\tau_f = \mu(P_0 + P_a) \quad (23)$$

In Equation 23, μ is given by the slope of the plot of τ_f against P_a, and P_0 is the value of the intercept at $P_a = 0$.

In contrast to the above technique which requires separate pull-out as well as hydrostatic pressure tests, a recent model [32, 58, 95] for determining μ and P_0 utilizes data from only one set of pull-out tests. In this method, the value of μ could be calculated from the additional energy expended in extracting a slightly tapered fibre, utilizing theoretical equations which accurately predicted and described the shape of the pull-out curve. The value for P_0 could then be determined by calculation using known relationships. This method can be applied to any system where a slightly tapered fibre test can be conducted.

5. Conclusion

This review has considered the interfacial properties of a fibre-reinforced composite. The role of the interfacial parameters in controlling the strength and toughness of the composite has been highlighted. The existing theories for predicting the stress distribution at the fibre–matrix interface and the applicability of these theories to real composite systems have been considered. In particular, the single-fibre pull-out test has been considered in detail, and the use of this test for determining the interfacial parameters has been examined. It is shown that the failure and pull-out process, and hence the properties of a fibre-reinforced composite, can be characterized in terms of its interfacial parameters.

It is apparent that although the existing theories can predict the general shape of the interfacial stress distribution, more remains to be done before the stress distribution in practical composite systems (which often have interphase regions between the fibre and the matrix) can be understood. Until the above aspects are properly understood, fibre-reinforced composites cannot be characterized properly and the full potential of composites as advanced materials will not be realized.

References

1. J. BOWYER and M. G. BADER, *J. Mater. Sci.* **7** (1972) 1315.
2. M. G. BADER and W. H. BOWYER, *Composites* **7** (1973) 150.
3. P. T. CURTIS, M. G. BADER and J. E. BAILEY, *J. Mater. Sci.* **13** (1978) 377.
4. P. E. CHEN, *Polym. Eng. Sci.* **11** (1971) 51.
5. V. R. RILEY and J. L. REDDAWAY, *J. Mater. Sci.* **3** (1968) 41.
6. R. E. LAVENGOOD, *Polym. Eng. Sci.* **12** (1972) 48.
7. B. F. BLUMENTRIT, B. T. VU and S. L. COOPER, *ibid.* **15** (1975) 428.

8. M. G. BADER and W. H. BOWYER, *J. Phys. D: Appl. Phys.* **5** (1972) 2215.
9. A. KELLY, *Proc. R. Soc.* **A282** (1964) 63.
10. D. C. PHILLIPS and A. S. TETELMAN, *Composites* **3** (1972) 216.
11. D. H. KAELBLE, *J. Adhesion* **5** (1973) 245.
12. J. N. KIRK, M. MUNRO and P. W. R. BEAUMONT, *J. Mater. Sci.* **13** (1978) 2197.
13. A. H. COTTRELL, *Proc. R. Soc.* **A282** (1964) 2.
14. A. KELLY, *ibid.* **A319** (1970) 95.
15. J. O. OUTWATER and M. C. MURPHY, in Proceedings of 24th ANTECH, New York, 1969 (SPI, New York, 1969) Paper 11C.
16. A. G. ATKINS, *J. Mater. Sci.* **10** (1975) 819.
17. J. COOK and J. E. GORDON, *Proc. R. Soc.* **A282** (1964) 508.
18. N. H. SUNG, T. J. JONES and N. P. SUH, *J. Mater. Sci.* **12** (1977) 239.
19. R. S. MILLMAN and J. G. MORLEY, *Mater. Sci. Engng* **23** (1976) 1.
20. L. J. BROUTMAN, *Polym. Eng. Sci.* **6** (1966) 1.
21. N. L. HANCOX, *J. Mater. Sci.* **10** (1975) 234.
22. M. G. BADER and J. F. COLLINS, in Proceedings of ICCM4, Tokyo, 1982 (Japan Society of Metals, Tokyo, 1982) p. 1067.
23. A. R. SANADI and M. R. PIGGOTT, *J. Mater. Sci.* **20** (1985) 421.
24. H. ISHIKAWA, T. W. CHOU and M. TAYA, *ibid.* **17** (1982) 832.
25. G. A. COOPER and A. KELLY, in "Interfaces in Composites", ASTM STP 452 (American Society for Testing and Materials, Philadelphia, 1969) p. 90.
26. B. HARRIS, J. MORLEY and D. C. PHILLIPS, *J. Mater. Sci.* **10** (1975) 2050.
27. B. HARRIS and A. O. ANKARA, *Proc. R. Soc.* **A359** (1978) 251.
28. R. K. MITTAL and V. B. GUPTA, *J. Mater. Sci.* **17** (1982) 3179.
29. A. KELLY and W. R. TYSON, *J. Mech. Phys. Solids* **13** (1965) 329.
30. W. R. TYSON and G. DAVIS, *Br. J. Appl. Phys.* **10** (1963) 199.
31. D. M. SCHUSTER and E. SCALA, American Institute of Aeronautics and Astronautics *J.* **6** (1968) 527.
32. C. Y. YUE and W. L. CHEUNG, *J. Mater. Sci.* in press.
33. A. KELLY and G. J. DAVIES, *Metall. Rev.* **10** (1965) 199.
34. L. T. DRAZL, M. J. RICH, M. F. KOENIG and P. A. LLOYD, *J. Adhesion* **16** (1983) 133.
35. H. L. COX, *Br. J. Appl. Phys.* **3** (1952) 72.
36. W. SACHSE, *Mater. Sci. Engng* **A126** (1990) 133.
37. N. J. PARRATT, *Rubb. Plast. Age* **41** (1960) 263.
38. M. J. FOLKES, in "Short Fibre Reinforced Thermoplastics" (Studies Press, London, 1982) p. 20.
39. A. N. NETRAVALI, L. T. T. TOPOLESKI, W. SACHSE and S. L. PHOENIX, *Compos. Sci. Techn.* **35** (1989) 13.
40. M. G. BADER and D. A. CLARKE, in Proceedings of 3rd European Conference on Composite Materials (ECCM-3), Bordeaux, March 1989, edited by A. R. Bunsell and A. R. Lamicq (Elsevier Applied Science, London, 1989) p. 79.
41. I. VERPOST, M. DESAEGER and R. KEUNINGS, in Proceedings of 3rd International Conference on Composite Interfaces (ICCI-III), Cleveland, May 1990, edited by H. Ishida (Elsevier Applied Science, New York, 1990) p. 653.
42. J. F. MANDELL, J. H. CHEN and F. J. McGARRY, *Int. J. Adhesion & Adhesives* **1** (1980) 40.
43. D. H. GRANDE, J. F. MANDELL and K. C. C. HONG, *J. Mater. Sci.* **23** (1988) 311.
44. D. L. CALDWELL, D. A. BABBINGTON and C. F. JOHNSON, in "Interfacial Phenomena in Composite Materials '89", edited by F. R. Jones (Butterworths, London, 1989) p. 44.
45. A. N. NETRAVALI, D. STONE, S. RUOFF and L. T. T. TOPOLESKI, *Compos. Sci. Techn.* **34** (1989) 289.
46. D. W. NICHOLSON, D. I. LIVINGSTON and G. S. F. RUSSELL, *Tire Sci. Techn.* **6** (1978) 114.
47. G. S. F. RUSSELL, D. I. LIVINGSTON and D. W. NICHOLSON, *Rubb. Chem. Techn.* **53** (1980) 950.
48. A. N. GENT, G. S. FIELDING-RUSSELL, D. I. LIVINGSTON and D. W. NICHOLSON, *J. Mater. Sci.* **16** (1981) 949.
49. R. C. DeVEKEY and A. J. MAJUMDAR, *Mag. Concr. Res.* **20** (1968) 229.
50. D. J. PINCHIN and D. TABOR, *J. Mater. Sci.* **13** (1978) 1261.
51. R. J. GRAY, *ibid.* **19** (1984) 1680.
52. R. BARTOS, *ibid.* **15** (1980) 3122.
53. P. L. WALTON and A. J. MAJUMDAR, *Composites* **6** (1975) 209.
54. P. B. BOWDEN, *J. Mater. Sci.* **5** (1970) 517.
55. N. HADJIS and M. R. PIGGOTT, *ibid.* **12** (1977) 358.
56. J. BOWLING and G. W. GROVES, *ibid.* **14** (1979) 431.
57. P. S. CHUA and M. R. PIGGOTT, *Compos. Sci. Techn.* **22** (1985) 107.
58. C. Y. YUE and W. L. CHEUNG, in Proceedings of 7th International Conference on Deformation, Yield and Fracture of Polymers, Cambridge, April 1988 (Plastics and Rubber Institute, London, 1988) p. 84.1.
59. B. MILLER, P. MURI and L. REBENFELD, *Compos. Sci. Techn.* **28** (1987) 17.
60. M. R. PIGGOTT, *Polym. Compos.* **8** (1987) 291.
61. P. S. CHUA and M. R. PIGGOTT, *Compos. Sci. Techn.* **22** (1985) 185.
62. W. V. TITOW and B. J. LANHAM, in "Reinforced Thermoplastics" (Applied Science, London, 1975) p. 5.
63. B. CUNNINGHAM, J. P. SARGENT and H. K. G. ASHBEE, *J. Mater. Sci.* **16** (1981) 620.
64. J. P. FAVRE, in "Interfacial Phenomena in Composite Materials '89", edited by F. R. Jones (Butterworths, London, 1989) p. 7.
65. U. GAUR and B. MILLER, *Compos. Sci. Techn.* **34** (1989) 35.
66. G. S. HOLISTER, in "Fibre Reinforced Materials" (Elsevier, London, 1966) p. 19.
67. J. OUTWATER and J. OGDEN, *Mod. Plast.* (1956) 56.
68. N. F. DOW, in GEC Missile and Space Division Report No. R63SD61 (GEC Interim Report, 1963).
69. B. W. ROSEN, in "Fibre Composite Materials" (ASM, Metals Park, Ohio, 1964) Ch. 3.
70. M. R. PIGGOTT, *Acta Metall.* **14** (1966) 1429.
71. C. T. CHON and C. T. SUN, *J. Mater. Sci.* **15** (1980) 931.
72. C. GALIOTIS, R. J. YOUNG, P. H. J. YEUNG and D. N. BATCHELDER, *ibid.* **19** (1984) 3640.
73. N. MELANITIS, P. TETLOW, C. GALIOTIS and C. K. L. DAVIES, in "Interfacial Phenomena in Composite Materials '89", edited by F. R. Jones (Butterworths, London, 1989) p. 97.
74. R. J. DAY, M. ZAKIKHANI, P. P. ANG and R. J. YOUNG, *ibid.* p. 121.
75. H. JAHANKHANI, C. VLATTAS and C. GALIOTIS, *ibid.* p. 125.
76. A. S. CARRARA and F. J. McGARRY, *J. Compos. Mater.* **2** (1968) 222.
77. Y. TERMONIA, *J. Mater. Sci.* **22** (1987) 504.
78. H. FUKUDA and K. KAWATA, *Fibre Sci. Techn.* **7** (1974) 129.
79. I. M. ALLISON and L. C. HOLLAWAY, *Br. J. Appl. Phys.* **18** (1967) 979.
80. A. OKAWARA, S. YONEMORI, A. KITSUNEZUKA and H. NISHIMURA, in Proceedings of 3rd International Conference on Composite Interfaces (ICCI-III), Cleveland, May 1990, edited by H. Ishida (Elsevier Applied Science, New York, 1990) p. 61.
81. J. F. GERARD, N. AMDOUNI, H. SAUTEREAU and J. P. PASCAULT, *ibid.* p. 441.
82. G. WACHINGER, *ibid.* p. 457.
83. J. L. THOMASON, in "Interfacial Phenomena in Composite Materials '89", edited by F. R. Jones (Butterworths, London, 1989) p. 171.
84. L. T. DRZAL, M. J. RICH, M. F. KOENIG and P. LLOYD, *J. Adhesion* **16** (1983) 133.
85. L. T. DRZAL, *Mater. Sci. Engng* **A126** (1990) 289.

86. T. BESSELL and J. B. SHORTALL, *J. Mater. Sci.* **10** (1975) 2035.
87. D. CAMPBELL and M. M. QAYYUM, *J. Polym. Sci., Polym. Phys. Edn* **18** (1980) 83.
88. R. H. BURTON and M. J. FOLKES, *Plast. Rubb. Process. Appl.* **3** (1983) 129.
89. H. ZENG and G. HE, *Scientia Sinica* **B27** (1984) 333.
90. C. Y. YUE and W. L. CHEUNG, *J. Mater. Sci.* **26** (1991) 870.
91. W. L. CHEUNG and C. Y. YUE, *Polym. Commun.* **31** (1990) 96.
92. L. J. BROUTMAN, in "Interfaces in Composites", ASTM STP 452 (American Society for Materials and Testing, Philadelphia, 1969) p. 27.
93. P. S. CHUA and M. R. PIGGOTT, *Compos. Sci. Techn.* **22** (1985) 33.
94. C. Y. YUE and W. L. CHEUNG, *J. Mater. Sci. Lett.* **10** (1991) 1335.
95. *Idem, J. Mater. Sci.* submitted.
96. L. B. GRESZCZUK, in "Interfaces in Composites", ASTM STP 452 (American Society for Materials and Testing, Philadelphia, 1969) p. 42.
97. P. LAWRENCE, *J. Mater. Sci.* **7** (1972) 1.
98. G. S. FIELDING-RUSSELL, D. I. LIVINGSTON and D. W. NICHOLSON, *Rubb. Chem. Techn.* **53** (1980) 950.
99. B. BETZ, *J. Mater. Sci.* **17** (1982) 691.
100. G. A. COOPER, *ibid.* **5** (1970) 645.
101. A. TAKAKU and R. G. C. ARRIDGE, *J. Phys. D: Appl. Phys.* **6** (1973) 2038.
102. R. J. GRAY, *J. Mater. Sci.* **19** (1984) 861.
103. M. J. PITKETHLY and J. B. DOBLE, *Composites* **21** (1990) 389.
104. J. K. WELLS and P. W. R. BEAUMONT, *J. Mater. Sci.* **23** (1988) 1274.
105. C. GURNEY and J. HUNT, *Proc. R. Soc.* **A299** (1967) 508.
106. H. STANG and S. P. SHAH, *J. Mater. Sci.* **21** (1986) 953.
107. K. KENDALL, *ibid.* **10** (1975) 1011.
108. C. K. Y. LEUNG and V. C. LI, *ibid.* **9** (1990) 1140.
109. C. A. COOPER and D. G. GLADMAN, in National Physical Laboratory IMS Report No. 8 (Internal Report, 1970).
110. J. K. WELLS and P. W. R. BEAUMONT, *J. Mater. Sci.* **20** (1985) 1275.

Received 19 March
and accepted 2 August 1991